

Constraints on the origin of cosmic rays from large scale anisotropy searches in data of the Pierre Auger Observatory

ROGERIO M. DE ALMEIDA¹ FOR THE PIERRE AUGER COLLABORATION².

¹ Universidade Federal Fluminense, EEIMVR, Volta Redonda, RJ, Brazil

² Full author list: http://www.auger.org/archive/authors_2013_05.html

auger_spokespersons@fnal.gov

Abstract: We update a search for large scale anisotropies in the distribution of arrival directions of cosmic rays detected above 10^{18} eV at the Pierre Auger Observatory as a function of both the right ascension and the declination. Within the systematic uncertainties, no significant deviation from isotropy is revealed. Upper limits on dipole and quadrupole amplitudes are updated under the hypothesis that any cosmic ray anisotropy is dominated by such moments in this energy range. These upper limits provide constraints on the production of cosmic rays above 10^{18} eV, since they allow us to challenge an origin from stationary galactic sources densely distributed in the galactic disk and emitting predominantly light particles in all directions.

Keywords: Pierre Auger Observatory, ultra-high energy cosmic rays, large-scale anisotropies

1 Introduction

The large scale distribution of arrival directions of Ultra-High Energy Cosmic Rays (UHECRs) as a function of the energy is a key observable to provide further understanding of their origin. As a natural signature of the escape of cosmic rays from the Galaxy [1, 2, 3], large scale anisotropies could be detected at energies below the ankle, a hardening of the energy spectrum located at $\simeq 4$ EeV. On the other hand, if UHECRs above 1 EeV have already a predominant extragalactic origin [4, 5, 6, 7], their angular distribution is expected to be isotropic to a high level. Thus, the study of large scale anisotropies at EeV energies would help in establishing whether the origin of UHECRs is galactic or extragalactic in this energy range.

A thorough search for large scale anisotropies in the distribution of arrival directions of cosmic rays detected above 10^{18} eV at the Pierre Auger Observatory was performed for several energy ranges in terms of dipoles and quadrupoles as a function of both the declination and the right ascension with no significant deviation from isotropy [8, 9]. Assuming that the eventual anisotropic component of the angular distribution of cosmic rays is dominated by dipole and quadrupole moments in this energy range, upper limits on their amplitudes were derived, challenging an origin of cosmic rays above 10^{18} eV from stationary galactic sources densely distributed in the galactic disk and emitting predominantly light particles in all directions. In this paper, we update this analysis. In section 2, we describe the data set and the procedure performed to control the exposure of the experiment below a 1% level while the results and the method used to derived them are presented in section 3.

2 Data set and control of the counting rate

The data set analyzed consists of 679,873 events recorded by the Surface Detector (SD) array of the Pierre Auger Observatory from 1 January 2004 to 31 December 2012, with zenith angles less than 55° and energies above 1 EeV. To ensure good reconstruction, an event is accepted only if all six nearest neighbours of the water-Cherenkov detector

with the highest signal were operational at the time of the event [10]. Based on this fiducial cut, any active water-Cherenkov detector with six active neighbours defines an active *elemental cell*. In these conditions, and above the energy at which the detection efficiency saturates, 3 EeV [10], the total exposure of the SD array is $28,130 \text{ km}^2 \text{ yr sr}$.

2.1 Influence of atmospheric conditions and geomagnetic field on shower size

Due to the steepness of the energy spectrum, any mild bias in the estimate of the shower energy with time or zenith angle can lead to significant distortions of the event counting rate above a given energy. It is thus critical to control the energy estimate in searching for anisotropies. The energy of each event is determined using the shower size at a reference distance of 1000 m, $S(1000)$. The geomagnetic field deflects the trajectories of charged particles of the shower and breaks the circular symmetry of the lateral spread of the particles inducing a dependence of the $S(1000)$ at a fixed energy in terms of the azimuthal angle. This dependence translates into azimuthal modulations of the estimated event counting rate at a given $S(1000)$ due to the steepness of the energy spectrum. The procedure followed to obtain an unbiased estimate of the shower energy consists in correcting measurements of shower signals for the influence of the geomagnetic field [11]

$$S_{geom}(1000) = \left[1 - g_1 \cos^{-g_2}(\theta) \sin^2(\vec{u} \cdot \vec{b}) \right] S(1000) \quad (1)$$

where $g_1 = (4.2 \pm 1.0) \times 10^{-3}$, $g_2 = 2.8 \pm 0.3$, and \vec{u} and $\vec{b} = \vec{B}/\|B\|$ denote the unit vectors in the shower direction and the geomagnetic field direction, respectively.

Besides, the atmospheric conditions also modify the shower sizes: (i) a greater (lower) pressure corresponds to a larger (smaller) matter overburden and implies that the shower is an advanced (old) stage when it reaches the ground level; (ii) the air density (related to temperature) changes the Molière radius and hence the lateral profiles of the showers. Similarly, the procedure to eliminate these variations consists in relating the $S(1000)$, measured at the

actual density ρ and pressure P , to the one $S_{atm}(1000)$ that would have been measured at reference values ρ_0 and P_0 , chosen as the average values at Malargue [12]

$$S_{atm}(1000) = [1 - \alpha_P(\theta)(P - P_0) - \alpha_\rho(\theta)(\rho_d - \rho_0) - \beta_\rho(\theta)(\rho - \rho_d)]S(1000), \quad (2)$$

where ρ_d is the average daily density at the time when the event was recorded and the coefficients, α_ρ and β_ρ , reflect respectively the impact of the variations of air density at long and short time scales and the variation of pressure on the shower size, α_P .

Once the influence on $S(1000)$ of weather and geomagnetic effects are accounted for, the shower signal is then converted to S_{38° , the value that would have been expected had the shower arrived at a zenith angle 38° , using the constant intensity cut method (CIC) [13]. This reference shower signal is finally converted into energy using a calibration curve based on hybrid events measured simultaneously by the SD array and the Fluorescence Detector (FD) telescopes through $E_{FD} = AS_{38^\circ}^B$, since the latter can provide a calorimetric measurement of the energy [14]. The parameters A and B are obtained from a fit to the data [15].

2.2 Exposure determination

In searching for anisotropies, it is also critical to know accurately the effective time-integrated collecting area for a flux from each direction of the sky, or in other words, the *directional exposure* ω of the Observatory. For each elemental cell, this is obtained through the integration over Local Sidereal Time (LST) α^0 of $x^{(i)}(\alpha^0) \times a_{cell}(\theta) \times \varepsilon(\theta, \varphi, E)$, with $x^{(i)}(\alpha^0)$ the total operational time of the cell (i) at LST α^0 , $a_{cell}(\theta) = 1.95 \cos \theta \text{ km}^2$ the geometric aperture of each elemental cell under incidence zenith angle θ [10], and $\varepsilon(\theta, \varphi, E)$ the detection efficiency under incidence zenith angle θ and azimuth angle φ at energy E .

The zenithal dependence of the detection efficiency $\varepsilon(\theta, \varphi, E)$ can be obtained directly from the data [8] based on the quasi-invariance of the zenithal distribution to large scale anisotropies for zenith angles less than $\sim 60^\circ$ and for any Observatory whose latitude is far from the poles of the Earth. Since $dN/d\sin^2(\theta)$ is uniform for full efficiency ($E > 3 \text{ EeV}$), any significant deviation from a uniform behavior in this distribution provides an empirical measurement of the zenithal dependence of the detection efficiency given by

$$\langle \varepsilon(\theta, \varphi, E) \rangle_\varphi = \frac{1}{\mathcal{N}} \frac{dN(\sin^2 \theta, E)}{d\sin^2 \theta} \quad (3)$$

where the notation $\langle \cdot \rangle_\varphi$ stands for the average over φ and the constant \mathcal{N} is the number of events that would have been observed at energy E and for any $\sin^2 \theta$ value in case of full efficiency for an energy spectrum $dN/dE = 40(E/\text{EeV})^{-3.27} \text{ km}^2 \text{ yr}^{-1} \text{ sr}^{-1} \text{ EeV}^{-1}$ as measured between 1 and 4 EeV [16].

Additional effects have an impact on ω , such as the azimuthal dependence of the efficiency due to geomagnetic effects, the corrections to both the geometric aperture of each elemental cell and the detection efficiency due to the tilt of the array, and the corrections due to the spatial extension of the array. A shower under any incident angles (θ, φ) and energy E triggers the SD array with a probability associated with its size which is a function of the azimuth

because of the geomagnetic effects. Considering that the energy that would have been obtained without correcting for geomagnetic effects is $E \times (1 + \Delta(\theta, \varphi))^B$,¹ to first order in $\Delta(\theta, \varphi)$, $\varepsilon(\theta, \varphi, E)$ can be estimated as:

$$\begin{aligned} \varepsilon(\theta, \varphi, E) &= \frac{1}{\mathcal{N}} \frac{dN(\sin^2 \theta, E(1 + \Delta(\theta, \varphi))^B)}{d\sin^2 \theta} \\ &\simeq \langle \varepsilon(\theta, \varphi, E) \rangle_\varphi + \frac{BE\Delta(\theta, \varphi)}{\mathcal{N}} \frac{\partial \langle \varepsilon(\theta, \varphi, E) \rangle_\varphi}{\partial E}. \end{aligned} \quad (4)$$

Thus, it is straightforward to implement the correction to the detection efficiency induced by geomagnetic effects from the knowledge of $\langle \varepsilon(\theta, \varphi, E) \rangle_\varphi$.

The slight tilt of the SD array gives rise to a small azimuthal asymmetry, and consequently, slightly modifies the directional exposure in a twofold way: changing the geometric factor ($\cos \theta$) of the projected surface under incident angles (θ, φ) for all energy ranges and slightly varying the detection efficiency with azimuth angle φ for energies below 3 EeV. The correction of the projected surface is performed replacing the $\cos \theta$ factor in a_{cell} by the geometric directional aperture per cell $a_{cell}^{(i)}$

$$\begin{aligned} a_{cell}^{(i)}(\theta, \varphi) &= 1.95 \hat{n} \cdot \hat{n}_\perp^{(i)} \\ &\simeq 1.95 [1 + \zeta^{(i)} \tan \theta \cos(\varphi - \varphi_0^{(i)})] \cos \theta \end{aligned} \quad (5)$$

where $\zeta^{(i)}$ and $\varphi_0^{(i)}$ are the zenith and azimuth angles of $\hat{n}_\perp^{(i)}$, the normal vector to each elemental cell. The variation of the detection efficiency with azimuth induced by the tilt of the array is because the effective separation between detectors for a given zenith angle depends on the azimuth, since the SD array seen by showers coming from the uphill direction is denser than those coming from the downhill direction. We showed in [8] that this change in the detection efficiency can be estimated by

$$\Delta \varepsilon_{tilt}(\theta, \varphi, E) = \frac{E^3 (E_{0.5}^3 - E_{0.5}^{tilt^3}(\theta, \varphi))}{(E^3 + E_{0.5}^3)(E^3 + E_{0.5}^{tilt^3}(\theta, \varphi))} \quad (6)$$

where $E_{0.5}^{tilt}(\theta, \varphi)$ is related to $E_{0.5}$, the zenithal-dependent energy at which $\varepsilon_{notilt}(E, \theta) = 0.5$, through

$$E_{0.5}^{tilt}(\cos \theta, \varphi) \simeq E_{0.5} \times [1 + \zeta^{eff} \tan \theta \cos(\varphi - \varphi_0^{eff})]^{3/2}. \quad (7)$$

Regarding the spatial extension of the array, the range of latitudes covered by all cells reaches $\simeq 0.5^\circ$ and induces a slightly different directional exposure between the cells located at the northern part of the array and the ones located at the southern part. This can be accounted for using the latitude of each cell $\ell_{cell}^{(i)}$ to perform the conversion from local angles (θ, φ) to equatorial coordinates (δ, α) in $a_{cell}(\theta(\alpha', \delta))$ before evaluating the integration to determine the exposure.

As in [18] the small modulation of the exposure in local sidereal time α^0 due to the variations of the operational time of each cell $x^{(i)}$ can be accounted for by re-weighting

1. The shorthand notation $\Delta(\theta, \varphi)$ stands for $g_1 \cos^{-g_2}(\theta) [\sin^2(\vec{u} \cdot \vec{b}) - \langle \sin^2(\vec{u} \cdot \vec{b}) \rangle_\varphi]$

the events with the number of elemental cells at the LST of each event k , $\Delta N_{\text{cell}}(\alpha_k^0)$. Accounting for all these effects, the resulting dependence of ω on declination is given by

$$\omega(\delta, E) = \sum_{i=1}^{n_{\text{cell}}} x^{(i)} \int_0^{24h} d\alpha' a_{\text{cell}}^{(i)}(\theta(\alpha', \delta)) \times [\varepsilon(\theta, \varphi, E) + \Delta\varepsilon_{\text{tilt}}(\theta, \varphi, E)], \quad (8)$$

where both θ and φ depend on the hour angle $\alpha' = \alpha - \alpha^0$, δ and $\ell_{\text{cell}}^{(i)}$. For a wide range of declinations between $\simeq -89^\circ$ and $\simeq -20^\circ$, the directional exposure is $\simeq 2,990 \text{ km}^2 \text{ yr}$ at 1 EeV, and $\simeq 4,186 \text{ km}^2 \text{ yr}$ for any energy above full efficiency. Then, at higher declinations, it smoothly falls to zero, with no exposure above 20° declination for zenith angles smaller than 55° .

3 Searches for large scale patterns

Any angular distribution over the sphere $\Phi(\mathbf{n})$ can be expanded in terms of spherical harmonics :

$$\Phi(\mathbf{n}) = \sum_{\ell \geq 0} \sum_{m=-\ell}^{\ell} a_{\ell m} Y_{\ell m}(\mathbf{n}), \quad (9)$$

where \mathbf{n} denotes a unit vector taken in equatorial coordinates. Due to the non-uniform and incomplete coverage of the sky at the Pierre Auger Observatory, the estimated coefficients $\bar{a}_{\ell m}$ are determined in a two-step procedure. First, from any event set with arrival directions $\{\mathbf{n}_1, \dots, \mathbf{n}_N\}$ recorded at LST $\{\alpha_1^0, \dots, \alpha_N^0\}$, the multipolar coefficients of the angular distribution coupled to the exposure function are estimated through :

$$\bar{b}_{\ell m} = \sum_{k=1}^N \frac{Y_{\ell m}(\mathbf{n}_k)}{\Delta N_{\text{cell}}(\alpha_k^0)}. \quad (10)$$

$\Delta N_{\text{cell}}(\alpha_k^0)$ corrects for the slightly non-uniform directional exposure in right ascension. Then, assuming that the multipolar expansion of the angular distribution $\Phi(\mathbf{n})$ is *bounded* to ℓ_{max} , the first $b_{\ell m}$ coefficients with $\ell \leq \ell_{\text{max}}$ are related to the non-vanishing $a_{\ell m}$ through :

$$\bar{b}_{\ell m} = \sum_{\ell'=0}^{\ell_{\text{max}}} \sum_{m'=-\ell'}^{\ell'} [K]_{\ell m}^{\ell' m'} \bar{a}_{\ell' m'}, \quad (11)$$

where the matrix K is entirely determined by the directional exposure :

$$[K]_{\ell m}^{\ell' m'} = \int_{\Delta\Omega} d\Omega \omega(\mathbf{n}) Y_{\ell m}(\mathbf{n}) Y_{\ell' m'}(\mathbf{n}). \quad (12)$$

Inverting Eqn. 11 allows us to recover the underlying $\bar{a}_{\ell m}$, with a resolution proportional to $([K^{-1}]_{\ell m}^{\ell m} \bar{a}_{00})^{0.5}$ [17]. As a consequence of the incomplete coverage of the sky, this resolution deteriorates by a factor larger than 2 each time ℓ_{max} is incremented by 1. With our present statistics, this prevents the recovery of each coefficient with good accuracy as soon as $\ell_{\text{max}} \geq 3$, which is why we restrict ourselves to dipole and quadrupole searches.

Assuming that the angular distribution of cosmic rays is modulated by a dipole and a quadrupole, we parameterize the intensity $\Phi(\mathbf{n})$ in any direction as :

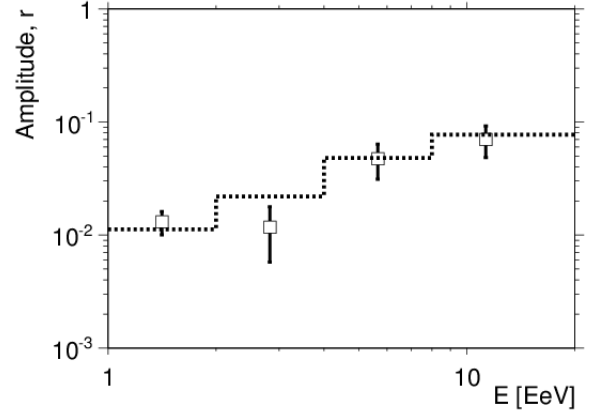


Fig. 1: Reconstructed amplitude of the dipole as a function of the energy. The dotted line stands for the 99% *C.L.* upper bounds on the amplitudes that would result from fluctuations of an isotropic distribution.

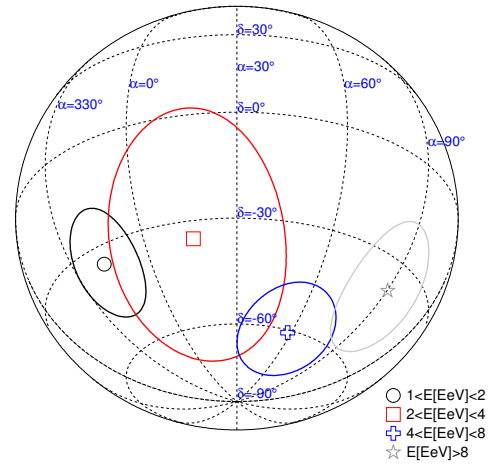


Fig. 2: Reconstructed declination and right-ascension of the dipole with corresponding uncertainties, as a function of the energy, in orthographic projection.

$$\Phi(\mathbf{n}) = \frac{\Phi_0}{4\pi} \left(1 + r \mathbf{d} \cdot \mathbf{n} + \lambda_+ (\mathbf{q}_+ \cdot \mathbf{n})^2 + \lambda_0 (\mathbf{q}_0 \cdot \mathbf{n})^2 + \lambda_- (\mathbf{q}_- \cdot \mathbf{n})^2 \right). \quad (13)$$

The dipole pattern is fully characterized by the dipole unit vector \mathbf{d} corresponding to declination δ_d , right ascension α_d and amplitude $r = (\Phi_{\text{max}} - \Phi_{\text{min}}) / (\Phi_{\text{max}} + \Phi_{\text{min}})$. Defining the amplitude $\beta \equiv (\lambda_+ - \lambda_-) / (2\lambda_+ + \lambda_-)$, which provides a measure of the maximal quadrupolar contrast in the absence of a dipole, any quadrupolar pattern can be fully described by two amplitudes (β, λ_+) and three angles : (δ_+, α_+) which define the orientation of \mathbf{q}_+ and (α_-) which defines the direction of \mathbf{q}_- in the orthogonal plane to \mathbf{q}_+ . The third eigenvector \mathbf{q}_0 is orthogonal to \mathbf{q}_+ and \mathbf{q}_- , and its corresponding eigenvalue is such as $\lambda_+ + \lambda_- + \lambda_0 = 0$. All these parameters are determined in a straightforward way from the spherical harmonic coefficients \bar{a}_{1m} and \bar{a}_{2m} .

First we consider a case of a pure dipole ($\lambda_{\pm,0} = 0$). The reconstructed amplitudes \bar{r} are shown in Fig. 1 as a function of the energy. The 99% *C.L.* upper bounds on the amplitudes that would result from fluctuations of

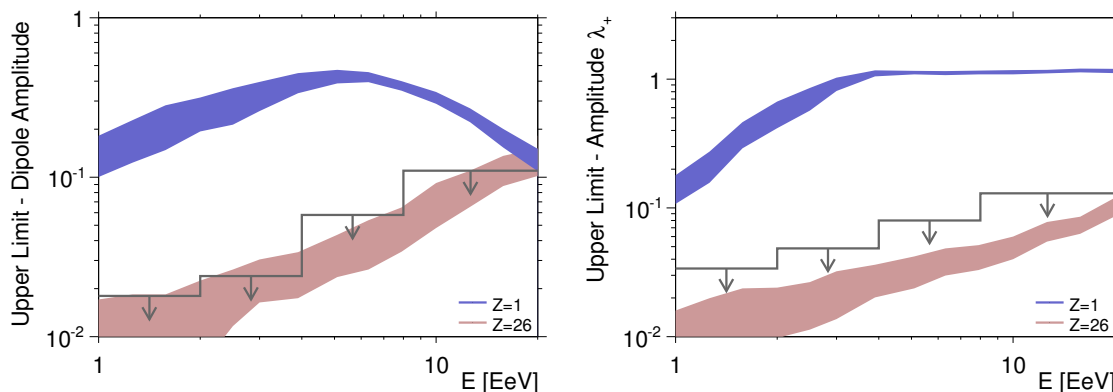


Fig. 3: 99% *C.L.* upper limits on dipole and quadrupole amplitudes as a function of the energy. Some generic anisotropy expectations from stationary galactic sources distributed in the disk are also shown, for various assumptions on the cosmic ray composition. The fluctuations (RMS) of the amplitudes due to the stochastic nature of the turbulent component of the magnetic field are sampled from different simulation data sets and are shown by the bands.

an isotropic distribution are indicated by the dotted line. One can see, similarly to the results from the analysis in [19], interesting hints for large scale anisotropies that will be important to further scrutinize with independent data. Figure 2 shows the corresponding reconstructed directions in orthographic projection with the associated uncertainties, as a function of the energy. Both angles are expected to be randomly distributed in the case of independent samples whose parent distribution is isotropic. It is thus interesting to note that all reconstructed declinations are in the equatorial southern hemisphere, and to note also the intriguing smooth alignment of the phases in right ascension as a function of the energy. In our previous report on first harmonic analysis in right ascension [18], we already pointed out this alignment, and stressed that such a consistency of phases in adjacent energy intervals is expected with smaller number of events than the detection of amplitudes standing-out significantly above the background noise in the case of a real underlying anisotropy. This motivated us to design a *prescription* aimed at establishing at 99% *C.L.* whether this consistency in phases is real, using the exact same analysis as the one reported in [18]. See [19] for an update of this analysis.

Upper bounds on the dipole and quadrupole amplitudes have been obtained at the 99% *C.L.* The bounds on the dipole amplitudes as a function of energy are shown in the left panel of Figure 3 along with generic estimates of the dipole amplitudes expected from stationary galactic sources distributed in the disk considering two extreme cases of single primaries: protons and iron nuclei. As an illustrative case we consider the Bisymmetric Spiral Structure (BSS) model with anti-symmetric halo with respect to the galactic plane [20] and a turbulent field generated according to a Kolmogorov power spectrum. Furthermore, assuming that the angular distribution of cosmic rays is modulated by a dipole and a quadrupole, the 99% *C.L.* upper bounds on the quadrupole amplitude λ_+ that could result from fluctuations of an isotropic distribution are shown in the right part of Figure 3 together with expectations considering the same astrophysical scenario described before. We will continue monitoring the contribution from higher moments in the flux.

While other magnetic field models, source distributions and emission assumptions must be considered, the example considered here illustrates the potential power of these

observational limits on the dipole anisotropy to exclude the hypothesis that the light component of cosmic rays comes from stationary sources densely distributed in the Galactic disk and emitting in all directions.

References

- [1] V. Ptuskin, *et al.*, *Astron. Astrophys* **268** (1993) 726
- [2] J. Candia, S. Mollerach, and E. Roulet, *JCAP* **0305** (2003) 003
- [3] G. Giacinti *et al.*, *JCAP* **07** (2012) 031
- [4] A. M. Hillas, *Phys. Lett.* **24A** (1967) 677
- [5] G. R. Blumenthal, *Phys. Rev. D* **1** (1970) 1596
- [6] V. S. Berezhinsky, A. Z. Gazizov and S. I. Grigorieva, *Phys. Rev. D* **74** (2006) 043005
- [7] V. S. Berezhinsky, S. I. Grigorieva and B. I. Hnatyk, *Astropart. Phys.* **21** (2004) 617625
- [8] The Pierre Auger Collaboration, *ApJS* **203** (2012) 34
- [9] The Pierre Auger Collaboration, *ApJL* **762** (2012) L13
- [10] The Pierre Auger Collaboration, *Nucl. Instr. and Meth. A* **613** (2010) 29
- [11] The Pierre Auger Collaboration, *JCAP* **11** (2011) 022
- [12] The Pierre Auger Collaboration, *Astropart. Phys.* **32** (2009) 89
- [13] J. Hershel *et al.*, *Phys. Rev. Lett.* **6** (1961) 22
- [14] The Pierre Auger Collaboration, *Phys. Rev. Lett.* **101** (2008) 061
- [15] V. Verzi, for the Pierre Auger Collaboration, paper 928, these proceedings.
- [16] The Pierre Auger Collaboration, *Phys. Lett. B* **685** (2010) 239
- [17] P. Billoir and O. Deligny, *JCAP* **02** (2008) 009
- [18] The Pierre Auger Collaboration, *Astropart. Phys.* **34** (2011) 627
- [19] I. Sidelnik, for the Pierre Auger Collaboration, paper 739, these proceedings.
- [20] M. S. Pshirkov *et al.*, *ApJ* **738** (2011) 192